Resolving the Future of Astronomy with Long-Baseline Interferometry
ASP Conference Series, Vol. 487
Creech-Eakman, Guzik, and Stencel

Starspot Imaging with the CHARA Array

J. R. Parks,[1] R. J. White,[1] G. H. Schaefer,[1,2] J. D. Monnier,[3] G. W. Henry,[4] H. A. McAlister,[1,2] and T. A. ten Brummelaar[2]

[1]*Department of Physics and Astronomy, Georgia State University, 29 Peachtree Center Avenue, Science Annex, Suite 400, Atlanta, GA 30303, USA; parksj@chara.gsu.edu, white@chara.gsu.edu*

[2]*Center for High Angular Resolution Astronomy, Georgia State University, Mount Wilson, CA, USA; schaefer@chara-array.edu*

[3]*Department of Astronomy, University of Michigan, 830 Dennison Bldg., 500 Church Street, Ann Arbor, MI, 48109,USA; monnier@umich.edu*

[4]*Center for Excellence in Information Systems, Tennessee State University, 3500 John Merritt Boulevard, Box 9501, Holland Hall Room 311, Nashville, TN, 37209, USA; gregory.w.henry@gmail.com*

Abstract. We present six H band interferometric images of cool starspots on the chromospherically active giant Lambda Andromedae. Images span ~75% of the rotational period with a cadence of ~1 week. The data were obtained using all six telescopes in the CHARA array with the MIRC beam combiner. Model solutions show cool starspots evenly distributed in longitude. The starspots have an average covering factor of 9.6% with a $\frac{T_{sp}}{T_{eff}} = 0.94$. We obtained consistent results between model solutions and MACIM reconstructions. The results of simulations testing model fidelity based on u,v sampling are presented. In addition, we present evidence interferometrically measured diameters are insensitive to cool starspot presence at an ~2.5% confidence level.

1. Introduction

Sunspots have been a ubiquitous feature of the Sun since their discovery in the early 1600s. A wealth of information concerning sunspot characteristics, formation and evolution has been discerned in the intervening centuries. However, understanding sunspots in the larger context of the Sun as a star has been missing until the last few decades. Through methods such as light curve inversion and Doppler imaging, we are beginning to understand the characteristics of cool starspots (Berdyugina 2005; Strassmeier 2009). However, as these are indirect methods, which rely on key assumptions, a method of direct observations is needed in order to confirm previous findings. In recent years, interferometric imaging has produced direct observations of rapidly rotating stellar surfaces, interacting binaries, and the eclipse of eta Aurigae by a companion's circumstellar disk (Monnier et al. 2007; Zhao et al. 2008; Kloppenborg et al. 2010; Zhao et al. 2010; Che et al. 2010). This work will present evidence of how interferometric imaging might provide the direct observations needed for cool starspots.

λ Andromedae (λ And) is a chromospherically active G8 giant as evidenced by strong Ca II H&K emission. As one of the brightest (V = 3.82) active giants with periodic (P∼54 days) significant variability (Δ V $\leq$ 0.20 mag), λ And makes an ideal target for interferometric imaging. This variability has allowed for previous predictions of starspot coverage and distribution through light curve inversion coupled with spectral line ratios (Donati et al. 1995; Frasca et al. 2008). λ And rotates too slowly (vsin$i$ = 6.5 km/s) for surface mapping via Doppler imaging.

2. Observations and Data Reduction

All interferometric observations, in the H band, were taken with the Center for High Angular Resolution Astronomy (CHARA) array. The Y-shaped array, consisting of six 1m telescopes, is capable of 15 non-redundant baselines, 20 closure phases and triple amplitudes. A spatial resolution down to ∼0.5 mas is possible with 331 m long baseline.

Between Aug. and Sept. 2010, 11 observations were obtained using all six telescopes taken four at a time. The observing strategy, aimed at capturing starspot motion, consisted of two observations on consecutive days separated by ∼ 1 week. This pattern was repeated throughout both months. The data from the consecutive days were combined in order to maximize the (u,v) coverage resulting in six total data sets. No data were combined with the 10 Sept. data.

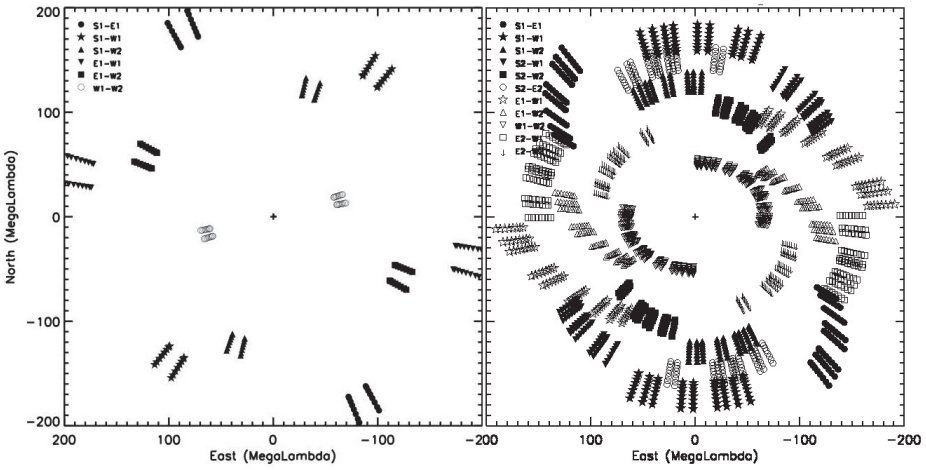

Figure 1. *Left:* (u,v) coverage of λ And on 17 August 2008. This is the typical (u,v) coverage obtained for all observations prior to August 2009. *Right:* (u,v) coverage of λ And on 18–19 August 2010. The data from the two nights are combined to further increase (u,v) sampling. This is the typical (u,v) coverage obtained for all observations in August and September 2010.

The Michigan InfraRed Combiner (MIRC) was used to combine the light from all four telescopes. Combining light from four telescopes yields visibilities on six baselines along with four closure phases and triple amplitudes. The light is passed through a prism (R ∼ 40), splitting the data into eight discrete spectral channels. We employ the standard MIRC data reduction pipeline to all observations (Monnier et al. 2007).

For the Aug. and Sept. 2010 observations, ~25% of the light from each telescope is picked off and sent a different quadrant on the detector. This provides real-time flux calibration, greatly increasing the measurement precision (Che et al. 2010). Final squared visibilities and triple products are obtained by calibrating system response with similar measurements from stars of known size.

Differential photometry, in the B and V bands, is obtained with the T3 0.40 m Automatic Photoelectric Telescope (APT) at Fairborn Observatory. The photometry is contemporaneous to our interferometric observations. However, Fairborn Observatory shuts down during August due to weather, when the majority of our CHARA was taken. The V band and (B-V) color photometry, along with dates of CHARA observations, is plotted in Figure 2.

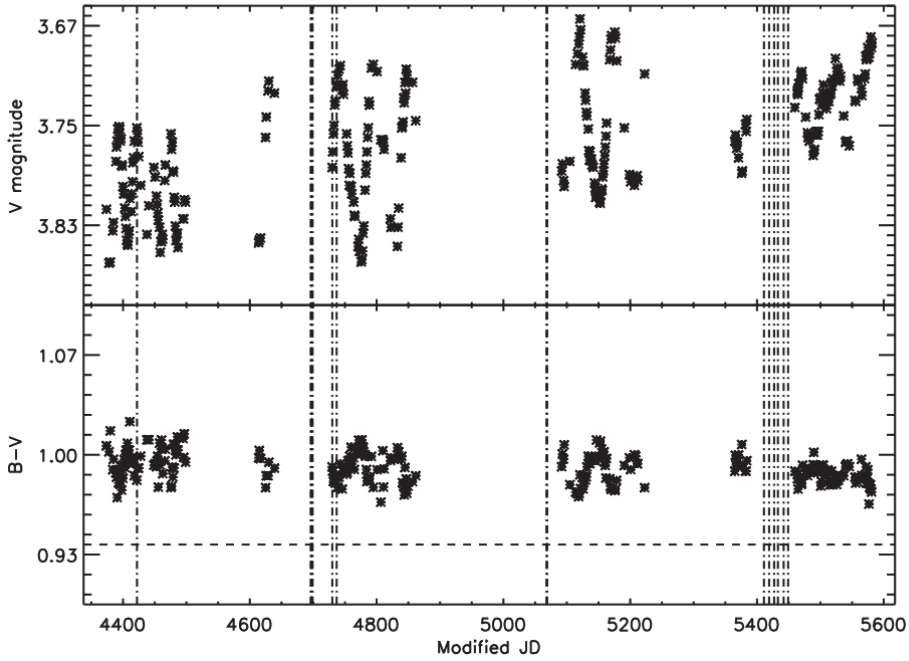

Figure 2. *Top:* V band photometry from 2007 to 2011. The variability of ~0.18 mag is presumed to be caused by cool starspots transiting the stellar disk. Varying variability amplitude points to starspot evolution on the timescale of months. The horizontal dashed line represents the $(B\text{-}V)_o$ for a G8 III. The vertical lines indicate the times of interferometric observations.

3. Analysis

3.1. Modeling and Imaging λ Andromedae

We analyze the data via two independent methods: image reconstruction and parametric modeling. Image reconstruction is done using the Markov-Chain Imager for Optical Interferometry (MACIM) (Ireland et al. 2006). The model surfaces are generated from

the data using a parametrized model. The final surface is found by minimizing the χ^2 between the observed data and data extracted from the trial models.

The parametrized model is a limb-darkened disk with the following free parameters: stellar size (θ), limb-darkening coefficient (α), covering factor (ϕ), starspot latitude (l), starspot longitude (b), and flux ratio (f) between the photosphere and starspot. Model squared visibilities and triple products are computed via a Fourier transform of a synthetic surface generated from a given set of parameters. A solution is found through χ^2 minimization between the model data and observed data using a downhill simplex method. The stellar parameters θ and α are found first by combining all obtained data sets. The solution is obtained by fitting only the first visibility lobe data with only θ and α as free parameters. The first lobe is insensitive to the presence of starspots. Once determined, both are held fixed when obtaining spot solutions. For each individual night, the full data set is employed to find the starspot parameters: ϕ, l, b and f. A two starspot solution was found for each data set.

MACIM employs a regularizer intended to minimize flux gradients over the stellar surface. This, in effect, produces the smoothest image that fits the observed data. The use of a prior image decreased the quality of fit; therefore, no priors were used for the presented reconstructions.

Figure 3 contains both the model results and reconstructions from 02 Aug. to 10 Sept. 2010. There appears to be agreement between the independently generated images for the same data set. However, more observations are needed to confirm this finding as inconsistencies do exist between the images. The modeled cool starspots have an average flux ratio of 0.789 ± 0.035, where the error is the standard deviation of the results. This corresponds to a temperature ratio between starspot and photosphere of 0.94. The average c_F, percentage of visible stellar disk, for the observed starspots is 9.6%. Frasca et al. (2008) found a temperature ratio of 0.815 and an average $c_F = 5.9\%$. Additionally, Frasca et al. (2008) found two spots only on one hemisphere whereas the models show a more even starspot distribution in longitude. The differences between the results may be related to when during λ And's overall ~11 year activity cycle both sets of observations were taken (Henry et al. 1995). The Frasca et al. (2008) observations may have occured during a period of large photometric amplitude sinusoidal variation, while the CHARA observations were taken during a smaller amplitude, chaotic period (see Figure 2).

3.2. Model Carlo Simulations

We conducted two different Monte Carlo simulations to answer the following questions: do cool starspots affect interferometric stellar diameter measurements, and how does increasing the (u,v) sampling improve model solutions?

To answer the first question, we generate 2000 synthetic stars with a random distribution of stellar and cool starspot properties. The input parameter ranges are consistent with those found in the literature (Berdyugina 2005). The (u,v) sampling is identical to the upper-left plot in Figure 2. Our result is interferometric diameter measurements are insensitive to starspots to an accuracy of ~2.5%. These results are valid even for spot configurations that drop the star's apparent magnitude by 0.27 mag. This has implications for the controversy between observed and modeled M dwarf radii (Ribas 2006).

The second question is explored by generating 2000 synthetic stars with different levels of (u,v) sampling. The trial stars are split evenly into four cases. Case 1 is two mid-evening observations with the Outer West array configuration. Case 2 is

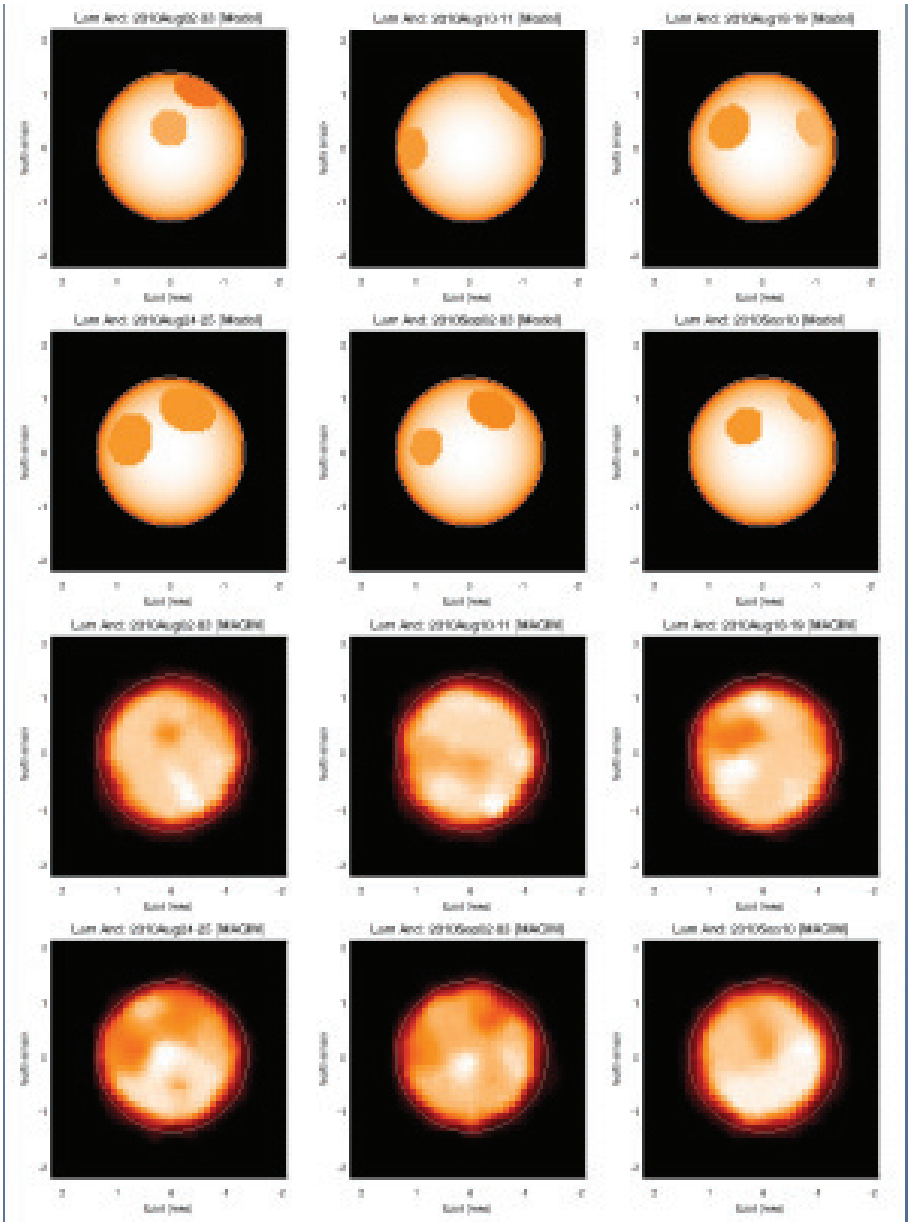

Figure 3. *Top*: two-spot models for six epochs between 02 Aug. and 10 Sept. 2010. The cadence between epochs is ∼7 days. *Bottom*: MACIM reconstructions for the same epochs. Considerable agreement exists between the models and reconstructions, expect for 10–11 Aug.

four observations observations with the same configuration. Case 3 combines the Case 2 observations with four observations employing the Inner West configuration. The observing cadence for these cases is 1 hour. Case 4 is identical to Case 3 except the observing cadence is now 30 minutes, allowing for 16 observations in total. We find an increase in (u,v) sampling improves the accuracy of determining starspot parame-

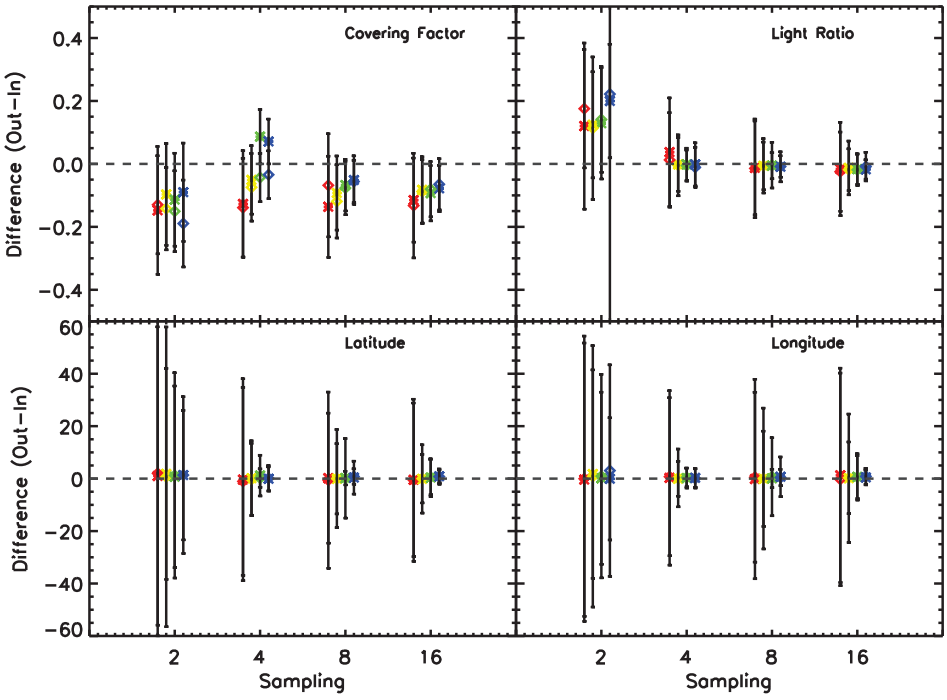

Figure 4. Starspot test results as a function of UV sampling. Data points indicate the mean difference between recovered parameters with corresponding input parameters. The error bars represent the 1σ dispersion between recovered and input parameters. *Red points*: mag bin 0.05-0.10. *Yellow points*: mag bin 0.10-0.15. *Green points*: mag bin 0.15-0.20. *Blue points*: mag bin 0.20-0.25.

ters. In addition, the errors associated with the starspot parameters decrease depending on how prominent the starspot appears. The plot in Figure 4 shows the results for our starspot parameter recovery test.

Acknowledgments. We thank the CHARA Array staff and MIRC team for their considerable assistance in obtaining these observations. We would also like to thank Fabien Baron for his expertise with image reconstruction.

References

Berdyugina, S. 2005, Living Review in Solar Physics, 2, 1

Che, X., Monnier, J. D., & Webster, S. 2010, in Society of Photo-Optical Instrumentation Engineers (SPIE) Conference Series, vol. 7734 of Presented at the Society of Photo-Optical Instrumentation Engineers (SPIE) Conference

Donati, J., Henry, G., & Hall, D. 1995, A&A, 293, 107

Frasca, A., Biazzo, K., Tas, G., Evren, S., & Lanzafame, A. 2008, A&A, 479, 557

Henry, G. W., Eaton, J. A., Hamer, J., & Hall, D. S. 1995, ApJS, 97, 513

Ireland, M. J., Monnier, J. D., & Thureau, N. 2006, in Society of Photo-Optical Instrumentation Engineers (SPIE) Conference Series, vol. 6268 of Presented at the Society of Photo-Optical Instrumentation Engineers (SPIE) Conference

Kloppenborg, B., Stencel, R., Monnier, J. D., Schaefer, G., Zhao, M., Baron, F., McAlister, H., Ten Brummelaar, T., Che, X., Farrington, C., Pedretti, E., Sallave-Goldfinger, P. J., Sturmann, J., Sturmann, L., Thureau, N., Turner, N., & Carroll, S. M. 2010, Nat, 464, 870. 1004.2464

Monnier, J. D., Zhao, M., Pedretti, E., Thureau, N., Ireland, M., Muirhead, P., Berger, J.-P., Millan-Gabet, R., Van Belle, G., ten Brummelaar, T., McAlister, H., Ridgway, S., Turner, N., Sturmann, L., Sturmann, J., & Berger, D. 2007, Science, 317, 342. 0706.0867

Ribas, I. 2006, in Astrophysics of Variable Stars, edited by C. Aerts & C. Sterken, vol. 349 of Astronomical Society of the Pacific Conference Series, 55

Strassmeier, K. G. 2009, A&A Rev., 17, 251

Zhao, M., Gies, D., Monnier, J. D., Thureau, N., Pedretti, E., Baron, F., Merand, A., ten Brummelaar, T., McAlister, H., Ridgway, S. T., Turner, N., Sturmann, J., Sturmann, L., Farrington, C., & Goldfinger, P. J. 2008, ApJ, 684, L95. 0808.0932

Zhao, M., Monnier, J. D., Pedretti, E., Thureau, N., Mérand, A., Ten Brummelaar, T., McAlister, H., Ridgway, S. T., Turner, N., Sturmann, J., Sturmann, L., Goldfinger, P. J., & Farrington, C. 2010, in Revista Mexicana de Astronomia y Astrofisica Conference Series, vol. 38 of Revista Mexicana de Astronomia y Astrofisica, vol. 27, 117